C. R. Chimie 22 (2019) 476–482

Contents lists available at ScienceDirect

Comptes Rendus Chimie

www.sciencedirect.com

Full paper / Mémoire

Tetra(*n*-butyl)ammonium salt of a ferrimagnetic complex based on mixed-valent dinuclear ruthenium pivalate and octacyanidotungstate(V)

Masahiro Mikuriya [a, *], Daisuke Yoshioka [a], Dominique Luneau [b], Shun Kawauchi [a], Dariusz Matoga [c], Janusz Szklarzewicz [c], Makoto Handa [d]

[a] Department of Applied Chemistry for Environment and Research Center for Coordination Molecule-Based Devices, School of Science and Technology, Kwansei Gakuin University, 2-1 Gakuen, Sanda 669-1337, Japan
[b] Univ Lyon, Université Claude-Bernard-Lyon-1, CNRS, Laboratoire des multimatériaux et interfaces, 69622 Villeurbanne, France
[c] Faculty of Chemistry, Jagiellonian University, Gronostajowa 2, 30-387 Kraków, Poland
[d] Department of Chemistry, Graduate School of Natural Science and Technology, Shimane University, 1060 Nishikawatsu, Matsue 690-8504, Japan

ARTICLE INFO

Article history:
Received 1 February 2019
Accepted 1 April 2019
Available online 7 May 2019

This work is dedicated to Prof. Michel Verdaguer on the occasion of his 75th birthday.

Keywords:
Ruthenium
Tungsten
Carboxylate
Cyanide
Crystal structure
Magnetic properties
Heterometallic compounds

ABSTRACT

A tetra (*n*-butyl)ammonium (n-Bu_4N^+) salt of Ru_2–W complex consisting of dinuclear ruthenium (II,III) pivalate, ($[Ru^{II}Ru^{III}(piv)_4]^+$) (Hpiv = pivalic acid), and octacyanidotungstate(V), $[n\text{-}Bu_4N][\{Ru^{II}Ru^{III}(piv)_4\}_2(H_2O)\{W^V(CN)_8\}]$ (**1**), was synthesized and characterized by elemental analysis, infrared spectra, and temperature dependence of magnetic susceptibilities (2–300 K). The crystal structure of **1** revealed a zigzag one-dimensional chain molecule along the *c* axis with alternating arrangement of $[Ru^{II}Ru^{III}(piv)_4]^+$ and $[W^V(CN)_8]^{3-}$, where another $[Ru^{II}Ru^{III}(piv)_4]^+$ unit is dangled from the $[W^V(CN)_8]^{3-}$ moiety. The magnetic susceptibilities and zero-field-cooled and field-cooled magnetization data showed that the present complex is ferrimagnetic with a T_c value of 5.5 K. The field dependence of magnetization exhibited a hysteresis with a coercive field of 150 Oe at 2 K.

1. Introduction

Dinuclear metal carboxylates with lantern-type or paddle-wheel–type core have a long history with copper acetate and a new aspect with ruthenium carboxylates, attracting much attention of many chemists for the past six decades because of their dinuclear core made-up by four carboxylato-bridges with metal–metal interaction or metal–metal bonding [1,2]. In case of dinuclear ruthenium carboxylates, mixed-valent $Ru^{II}Ru^{III}$ state is more stable and gives rise to paramagnetic property with a 3/2 spin system [1,3–5]. We have brought this 3/2 spin system into focus as a spin source for molecular magnetic materials [5–18,24–31]. To develop these magnetic materials, we and Miller et al. introduced cyanidometalate linking ligands into dinuclear ruthenium carboxylates and obtained mixed-metal complexes of dinuclear ruthenium(II,III) carboxylates with dicyanidoargentate(I) ($Ag(CN)_2^-$) [27], tetracyanidonickelate(II) ($Ni(CN)_4^{2-}$) [23,26], tetracyanidoplatinate(II) ($Pt(CN)_4^{2-}$) [28,29], and hexacyanidocobaltate(III) ($Co(CN)_6^{3-}$) [17,19–22]. These mixed-metal compounds have paramagnetic properties with a weak antiferromagnetic interaction between 3/2

* Corresponding author.
E-mail address: junpei@kwansei.ac.jp (M. Mikuriya).

https://doi.org/10.1016/j.crci.2019.04.001

spins of dinuclear ruthenium units through the diamagnetic cyanidometalate groups. On the other hand, mixed-metal compounds with hexacyanidoferrate(III) ($Fe(CN)_6^{3-}$) [17,19–22], hexacyanidochromate(III) ($Cr(CN)_6^{3-}$) [19–22], and octacyanidotungstate(V) ($W(CN)_8^{3-}$) have a considerable magnetic interaction between the $Ru^{II}Ru^{III}$ $S = 3/2$ spins and cyanidometalate $S = 1/2$ spin, resulting in a ferrimagnetic interaction [24,25,30]. Specifically, mixed-metal compound $[\{Ru^{II}Ru^{III}(piv)_4\}_3(H_2O)\{W^V(CN)_8\}]$ of ruthenium pivalate $[Ru^{II}Ru^{III}(piv)_4]^+$ (Hpiv = pivalic acid) with octacyanidotungstate $[W^V(CN)_8]^{3-}$ showed a high T_c value of 44 K, whereas an analogous mixed-metal compound $[PPh_4]_2[\{Ru^{II}Ru^{III}(piv)_4\}\{W^V(CN)_8\}]$ with octacyanidotungstate and tetraphenylphosphonium ion did not show a ferrimagnetic behavior [25]. This observation suggests that the presence of cation, here, tetraphenylphosphonium, may be a clue to obtaining a new phenomenon in our systems. Thus, we introduced a different cation, tetraethylammonium, to ruthenium pivalate and obtained the mixed-metal compound $[Et_4N][\{Ru^{II}Ru^{III}(piv)_4\}_2\{W^V(CN)_8\}]$ [30]. Intriguingly, this compound showed a ferrimagnetic interaction with a high T_c of 80 K. However, it was very difficult to obtain single crystals for this compound to determine the crystal structure by X-ray crystallography, and we could not reveal the molecular structure of this interesting compound. In this study, we synthesized new mixed-metal complex of ruthenium(II)–ruthenium(III) pivalate and octacyanidotungstate(V) by using tetra (*n*-butyl)ammonium $[n\text{-}Bu_4N]^+$ ion as a cation in the hope of obtaining single crystals suitable for X-ray crystallography. The isolated mixed-metal compound $[n\text{-}Bu_4N][\{Ru^{II}Ru^{III}(piv)_4\}_2(H_2O)\{W^V(CN)_8\}]$ (**1**) was characterized by using elemental analysis, infrared and UV–vis spectroscopies, and temperature dependence of magnetic susceptibilities (Fig. 1). The crystal structure of **1**·H_2O was determined by the single-crystal X-ray diffraction method.

2. Results and discussion

Analytical C, H, and N data of the isolated complex are in agreement with the 1:2:1 of $[n\text{-}Bu_4N]^+$:$[Ru^{II}Ru^{III}(piv)_4]^+$:$[W(CN)_8]^{3-}$ formulation with $[n\text{-}Bu_4N][\{Ru^{II}Ru^{III}(piv)_4\}_2(H_2O)\{W^V(CN)_8\}]$ (**1**) like the case of $[Et_4N][\{Ru^{II}Ru^{III}(piv)_4\}_2\{W^V(CN)_8\}]$ [30]. IR data showed a strong ν(CN) band of $W^V(CN)_8^{3-}$ moiety at 2145 cm^{-1} and two COO stretching bands at 1488 and 1420 cm^{-1} with the difference in energy characteristic of *syn–syn* bridging carboxylate [32].

As shown in Fig. 2, the diffuse reflectance spectrum of **1** showed a broad band at 1120 nm in the near-infrared region. The broad band can be assigned to the δ (Ru2) → δ*(Ru2) transition band [3–5] and showed a red shift as compared with that of $[Ru_2(piv)_4(H_2O)_2]BF_4$ (990 nm), suggesting the axial coordination of the cyanido group of $W(CN)_8^{3-}$ moiety [12].

Single-crystal X-ray structure analysis was performed for 1·H_2O. The crystallographic asymmetric unit contains one $[n\text{-}Bu_4N]^+$ cation, one $[\{Ru^{II}Ru^{III}(piv)_4\}_2(H_2O)\{W^V(CN)_8\}]^-$ anion, and one water molecule. The ORTEP (Oak Ridge thermal-ellipsoid plot program) drawing of the $[\{Ru^{II}Ru^{III}(piv)_4\}_2(H_2O)\{W^V(CN)_8\}]^-$ anion is shown in Fig. 3. The coordination number of each ruthenium atom is 6, including the metal–metal bond, and the coordination geometry is an axially elongated octahedron. The Ru–Ru [2.287(8)–2.300(10) Å] and Ru–O (carboxylato) [2.014(7)–2.056(7) Å], and Ru–N [2.275(10)–2.286(11) Å] distances are within the normal ranges as the mixed-valent dinuclear $Ru^{II}Ru^{III}$ carboxylates [5,25]. On the other hand, the coordination number of the tungstate atom is 8 and the coordination geometry can be regarded as a distorted bicapped trigonal prism based on the polytopal analysis ($\delta_1 = 16.4°$, $\delta_2 = 5.9°$, $\delta_3 = 51.7°$, $\delta_4 = 49.9°$, $\phi_1 = 24.4°$, $\phi_2 = 19.1°$) [25]. The W–C bond distances [2.173(9)–2.193(10) Å] are comparable to those of μ_3-$[W^V(CN)_8]^{3-}$ [25]. In the $[\{Ru^{II}Ru^{III}(piv)_4\}_2(H_2O)\{WV(CN)_8\}]^-$ anion, one crystallographically independent $[WV(CN)_8]^{3-}$ is bound to two $[Ru^{II}Ru^{III}(piv)_4]^+$ units (Ru1–$Ru1^i$ and Ru2–$Ru2^{ii}$), which have a crystallographical inversion center of symmetry and one crystallographically independent $[Ru^{II}Ru^{III}(piv)_4]^+$ unit (Ru3–Ru4). Of the three $[Ru^{II}Ru^{III}(piv)_4]^+$ units, two $[Ru^{II}Ru^{III}(piv)_4]^+$ (Ru1–$Ru1^i$ and Ru2–$Ru2^{ii}$) units are further connected by another $[W^V(CN)_8]^{3-}$ to form a zigzag one-dimensional (1D) chain along the *c* axis with alternating arrangement of $[Ru^{II}Ru^{III}(piv)_4]^+$ cation and $[W^V(CN)_8]^{3-}$ anion, where the third $[Ru^{II}Ru^{III}(piv)_4]^+$ (Ru3–Ru4) unit is attached to the $[W^V(CN)_8]^{3-}$ ion. One of the axial position of the third $[Ru^{II}Ru^{III}(piv)_4]^+$ unit is occupied by a water molecule (O17), which acts as a terminal ligand with the Ru4–O17 distance of 2.272 (9) Å. This coordinated water molecule is hydrogen bonded with the crystal water molecule (O17–H···O18) and the coordinated CN group (O17–H···$N7^{iii}$) (Table 3). The water molecule for O17 is an aqua ligand, whereas the water molecule of O18 is a water molecule of crystallization. The crystal water molecule is

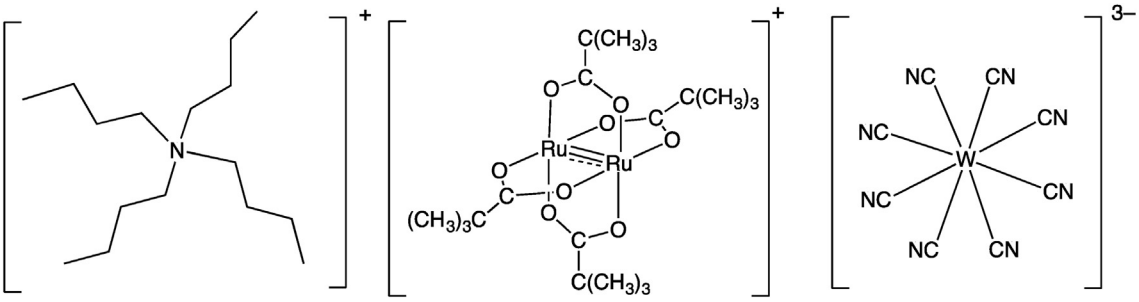

Fig. 1. Chemical structures of $[n\text{-}Bu_4N]^+$, $[Ru^{II}Ru^{III}(piv)_4]^+$ (two kinds of units), and $[W^V(CN)_8]^{3-}$.

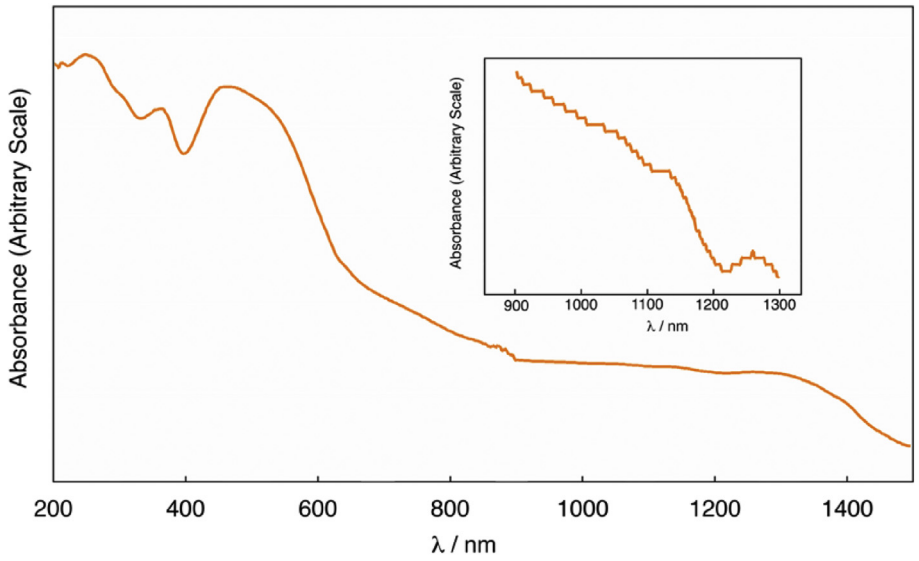

Fig. 2. Diffused reflectance spectra of **1**.

also hydrogen-bonded to the coordinated CN nitrogen atom (O18–H···N6^{iii}). If the hydrogen bonds between the O17 and N7^{iii} atoms are included, the chain molecules are connected to form a 2D supramolecular sheet constructed by 32-membered rings [–CN–Ru_2–NC–W–CN–Ru_2–OH–NC–W–CN–Ru_2–NC–W–CN–Ru_2–OH–NC–W–], as shown in Fig. 4. In the crystal, the tetra (*n*-butyl)ammonium ions, [*n*-Bu_4N]$^+$, enter the interstice, separating the two-dimensional sheets (Fig. 5) (see Table 2).

Magnetic susceptibility measurements were carried out in the temperature range of 2–300 K. The magnetic data of **1** are shown in Fig. 6 in the form of $\chi_M T$-*T* plots, where χ_M is the molar magnetic susceptibility per $(Ru^{II}Ru^{III})_2W^V$ unit. As shown in Fig. 6, $\chi_M T$ at 300 K is 1.17 cm^3 K mol^{-1} corresponding to the effective magnetic moment of 3.06 μB, which is definitely lower than the spin-only value ($\mu_{S.O.}$ = $(33)^{1/2}$ = 5.74 μB) expected for magnetically isolated two dinuclear $Ru^{II}Ru^{III}$ $S = 3/2$ ions (each dinuclear $Ru^{II}Ru^{III}$ unit has an $S = 3/2$ spins because of the metal–metal bonding [5]) and a W^V $S = 1/2$ ion (theoretical value for $g = 2$). As the temperature is lowered, $\chi_M T$ gradually increases up to a value of 6.52 cm^3 K mol^{-1} at 26 K then below it rapidly increases until 6 K with a maximum of 40.5 cm^3 K mol^{-1} (18.00 μB) at 6 K, and then decreasing rapidly down to 17.68 cm^3 K mol^{-1} (11.90 μB) at 2 K. The magnetic behavior

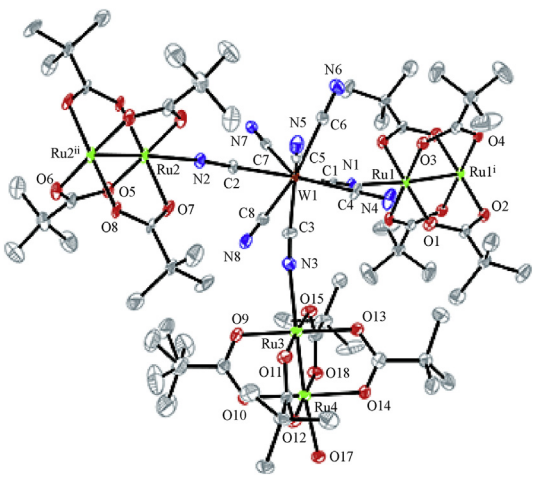

Fig. 3. ORTEP drawing of the molecular structure for [{$Ru^{II}Ru^{III}(piv)_4$}$_2$(H_2O){$W^V(CN)_8$}]$^-$ moiety of **1**·H_2O, showing the thermal ellipsoids at the 50% probability level. Hydrogen atoms are omitted for clarity.

Table 1
Crystal and experimental data.

Chemical formula: $C_{64}H_{112}N_9O_{18}Ru_4W$	
Formula weight = 1883.75	
T = 90 K	
Crystal system: triclinic	Space group $P\bar{1}$
a = 12.08 (5) Å	α = 92.62 (10)°
b = 13.97 (6) Å	β = 92.21 (11)°
c = 26.21 (11) Å	γ = 103.52 (7)°
V = 4289 (31) Å^3	
Z = 2	
D_x = 1.459 g/cm^3	
Radiation: Mo Kα (λ = 0.71073 Å)	
μ(Mo Kα) = 2.086 mm^{-1}	
F (000) = 1906	
Crystal size = 0.04 × 0.40 × 0.52 mm^3	
No. of reflections collected = 26,265	
No. of independent reflections = 19,177	
θ range for data collection: 1.50–28.57°	
Data/restraints/parameters = 19,117/0/926	
Goodness-of-fit on F^2 = 0.993	
R indices [$I > 2\sigma(I)$]: $R1$ = 0.0526, $wR2$ = 0.1247	
R indices (all data): $R1$ = 0.0815, $wR2$ = 0.1403	
Measurement: Bruker Smart APEX CCD diffractometer	
Program system: SHELXTL	
Structure determination: intrinsic phasing (SHELXT-2014/4)	
Refinement: full-matrix least-squares (SHELXL-2014/7)	
CCDC deposition number: 1894536	

Table 2
Selected bond distances (Å) and angles (°).

W1–C1	2.193 (10)
W1–C2	2.186 (10)
W1–C3	2.179 (10)
W1–C4	2.175 (9)
W1–C5	2.191 (9)
W1–C6	2.184 (9)
W1–C7	2.180 (9)
W1–C8	2.173 (9)
Ru1–Ru1^{i}	2.298 (9)
Ru2–Ru2^{ii}	2.300 (10)
Ru3–Ru4	2.287 (8)
Ru1–O1	2.023 (8)
Ru1–O2^{i}	2.036 (8)
Ru1–O3	2.017 (7)
Ru1–O4^{i}	2.049 (8)
Ru1–N1	2.286 (11)
Ru2–O5	2.031 (8)
Ru2–O6^{ii}	2.024 (8)
Ru2–O7	2.023 (8)
Ru2–O8^{ii}	2.033 (8)
Ru2–N2	2.280 (11)
Ru3–O9	2.033 (8)
Ru3–O11	2.056 (7)
Ru3–O13	2.025 (8)
Ru3–O15	2.043 (7)
Ru3–N3	2.275 (10)
Ru4–O10	2.040 (8)
Ru4–O12	2.014 (7)
Ru4–O14	2.032 (8)
Ru4–O16	2.018 (7)
Ru4–O17	2.272 (9)
C1–W1–C2	144.5 (3)
C1–W1–C3	112.6 (2)
C1–W1–C4	69.7 (3)
C1–W1–C5	141.1 (2)
C1–W1–C6	79.6 (3)
C1–W1–C7	74.7 (2)
C1–W1–C8	78.0 (2)
C2–W1–C3	84.0 (3)
C2–W1–C4	145.6 (2)
C2–W1–C5	71.7 (3)
C2–W1–C6	105.6 (3)
C2–W1–C7	73.4 (2)
C2–W1–C8	78.4 (2)
C3–W1–C4	74.7 (3)
C3–W1–C5	76.4 (3)
C3–W1–C6	144.4 (3)
C3–W1–C7	141.4 (2)
C3–W1–C8	71.2 (3)
C4–W1–C5	77.2 (4)
C4–W1–C6	79.2 (3)
C4–W1–C7	138.1 (3)
C4–W1–C8	118.1 (3)
C5–W1–C6	74.5 (3)
C5–W1–C7	122.9 (3)
C5–W1–C8	137.6 (3)
C6–W1–C7	73.2 (4)
C6–W1–C8	143.9 (2)
C7–W1–C8	73.8 (4)
O1–Ru1–O2^{i}	178.60 (16)
O1–Ru1–O3	89.6 (4)
O1–Ru1–O4^{i}	90.9 (3)
O1–Ru1–N1	91.28 (19)
O1–Ru1–Ru1^{i}	89.52 (17)
O2i–Ru1–O3	90.2 (3)
O2i–Ru1–O4^{i}	89.3 (3)
O2–Ru1–N1^{i}	90.07 (19)
O2i–Ru1–Ru1^{i}	89.10 (16)
O3–Ru1–O4^{i}	178.64 (15)
O3–Ru1–N1	84.5 (2)
O3–Ru1–Ru1^{i}	88.9 (2)

Table 2 (*continued*)

O4i–Ru1–N1	96.8 (2)
O4i–Ru1–Ru1^{i}	89.8 (2)
N1–Ru1–Ru1^{i}	173.35 (13)
O5–Ru2–O6^{ii}	178.42 (15)
O5–Ru2–O7	90.1 (3)
O5–Ru2–O8^{ii}	89.5 (3)
O5–Ru2–N2	94.5 (2)
O5–Ru2–Ru2^{ii}	89.78 (17)
O6^{ii}–Ru2–O7	90.4 (3)
O6^{ii}–Ru2–O8^{ii}	89.9 (3)
O6^{ii}–Ru2–N2	87.02 (19)
O6^{ii}–Ru2–Ru2^{ii}	88.75 (17)
O7–Ru2–O8^{ii}	178.57 (15)
O7–Ru2–N2	84.0 (2)
O7–Ru2–Ru2^{ii}	88.53 (17)
O8^{ii}–Ru2–N2	97.4 (2)
O8^{ii}–Ru2–Ru2^{ii}	90.10 (10)
N2–Ru2–Ru2^{ii}	171.38 (14)
O9–Ru3–O11	90.6 (3)
O9–Ru3–O13	179.17 (15)
O9–Ru3–O15	91.0 (4)
O9–Ru3–N3	90.0 (2)
O9–Ru3–Ru4	89.1 (2)
N3–Ru3–Ru4	170.87 (13)
O10–Ru4–O12	90.3 (4)
O10–Ru4–O14	178.43 (17)
O10–Ru4–O16	90.5 (4)
O10–Ru4–O17	95.6 (2)
O10–Ru4–Ru3	89.8 (2)
O12–Ru4–O14	89.6 (4)
O12–Ru4–O16	178.62 (17)
O12–Ru4–O17	90.7 (3)
O12–Ru4–Ru3	89.6 (3)
O14–Ru4–O16	89.6 (4)
O14–Ru4–O17	86.0 (2)
O14–Ru4–Ru3	88.7 (2)
O16–Ru4–O17	88.1 (3)
O16–Ru4–Ru3	91.5 (3)
O17–Ru4–Ru3	174.65 (13)

Symmetry codes: (i) $(1-x, 1-y, -z)$; (ii) $(1-x, 1-y, 1-z)$.

is characteristic of ferrimagnetic behavior because of antiferromagnetic interaction between $Ru^{II}Ru^{III}$ and W^{V} ions through the cyanido bridges. The first magnetization curves at different temperatures (Fig. 7) show that the magnetization increases but never reaches the expected saturation value for the ferromagnetically coupled system ($S_{total} = 4$, $M_{sat} = 8$ μB). However, the variation in the magnetization is different above and below 5 K, suggesting the onset of magnetic ordering. The zero-field-cooled (ZFC) and field-cooled (FC) magnetizations, $M(T)$ZFC and $M(T)$FC, respectively, rise below 5.5 K (Fig. 8), indicative of an onset magnetic transition with T_c at 5.5 K. Below 5.5 K, M(T)ZFC decreases presumably because of a domain wall freezing, whereas $M(T)$FC continues to increase up to 2 K. Below T_c, the field dependence of the magnetization $M(H)$ shows magnetic hysteresis as shown in Fig. 9. The hysteresis curves at different temperatures show that the coercive

Table 3
Hydrogen-bonding geometry (Å, °).

D–H···A	D–H (Å)	H···A (Å)	D···A (Å)	D–H···A (°)
O17–H17E···O18	0.90 (8)	1.85 (8)	2.746 (11)	174 (7)
O17–H17D···N7^{iii}	0.69 (7)	2.12 (7)	2.790 (11)	163 (8)
O18–H18D···N6^{iii}	0.64 (8)	2.40 (8)	3.000 (11)	158 (10)

Symmetry code: (iii) $(x, y-1, z)$.

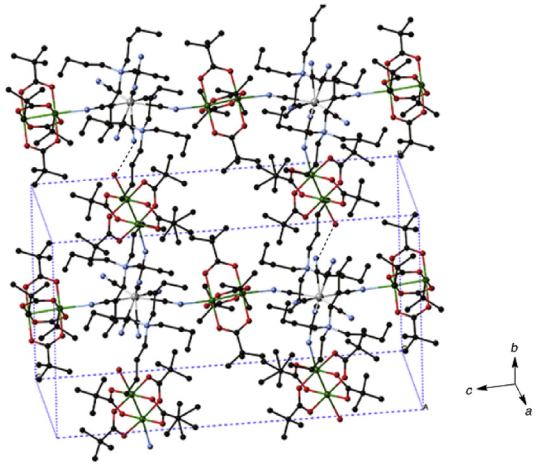

Fig. 4. Packing diagram for **1**·H_2O, showing hydrogen bonding with dotted lines.

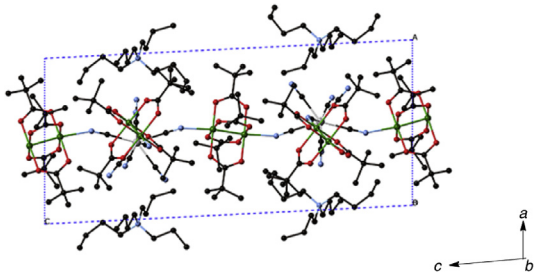

Fig. 5. Packing diagram of **1**·H_2O, showing the $[n\text{-}Bu_4N]^+$ moieties and 2D supramolecular Ru_2W sheet.

field increases as the temperature decreases as expected for a magnet. The coercive field is about 150 Oe at 2 K. In case of $[\{Ru^{II}Ru^{III}(piv)_4\}_3(H_2O)\{W^V(CN)_8\}]$, definitely high T_c value (44 K) and large coercive field (5600 Oe at 5 K) were observed [25]. In $[\{Ru^{II}Ru^{III}(piv)_4\}_3(H_2O)\{W^V(CN)_8\}]$, the 2D sheet structure was constructed by assembling of 28-membered rings made up from four $Ru_2(piv)_4^+$ units and four $W(CN)_8^{3-}$ units with alternating arrangement of

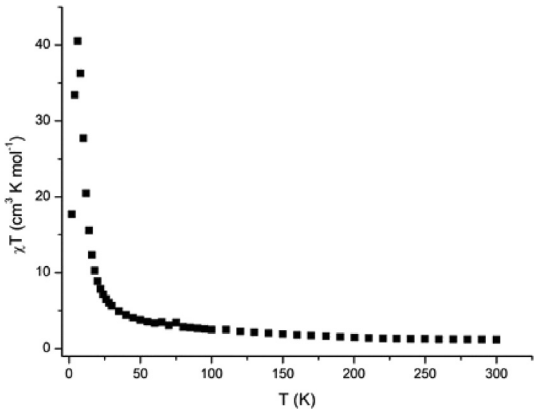

Fig. 6. Temperature dependence of $\chi_M T$ of **1**.

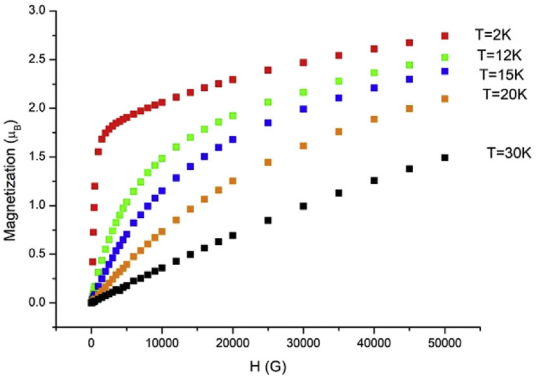

Fig. 7. Field dependence of the magnetization at different temperatures for **1**.

$[Ru^{II}Ru^{III}(piv)_4]^+$ and $[W^V(CN)_8]^{3-}$. The high T_c and large coercive field may be ascribed to the 2D sheet structure and the large anisotropies of the diruthenium cations and tungstate ions. We can suppose this kind of 2D sheet structure for the $[Et_4N][\{Ru^{II}Ru^{III}(piv)_4\}_2\{W^V(CN)_8\}]$ complex, which has the high T_c value of 80 K and large coercive

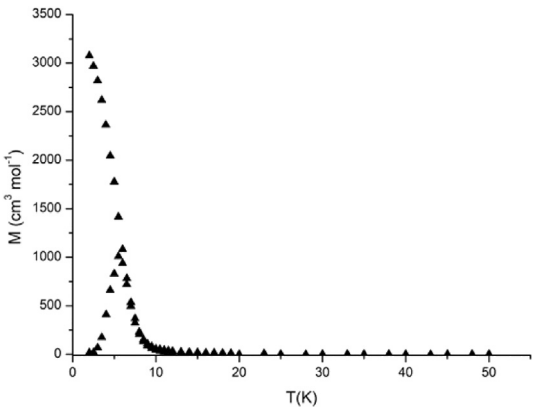

Fig. 8. ZFC (upper) and FC (lower) magnetization curves measured in 15 G for **1**.

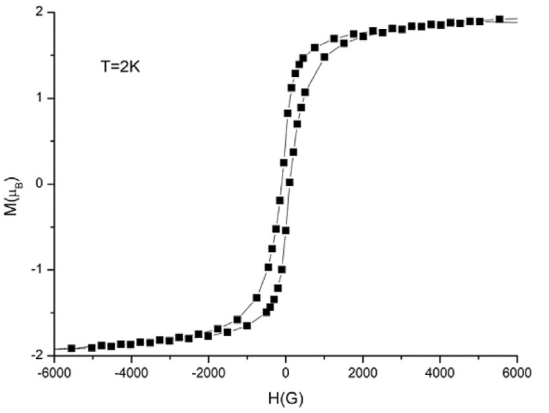

Fig. 9. Magnetic hysteresis loop at 2 K for **1**.

field of 17,000 Oe at 5 K [30], because the 2D sheet structure was observed for the similar 2:1 mixed–metal complex, $[\{Ru^{II}Ru^{III}(CH_3COO)_4\}_2Pt(CN)_4]\cdot 2H_2O$ [29]. On the other hand, the present complex is essentially 1D chain structure, although the 2D sheet structure can be considered with hydrogen bonding between the O17 (water molecule) and $N7^{iii}$ (coordinated CN group) atoms. From the point of view of magnetic interaction, the present complex can be considered as 1D ferrimagnetic chain complex, resulting in the low T_c value and small coercive field.

3. Conclusion

A new mixed-metal complex $[n\text{-}Bu_4N][\{Ru^{II}Ru^{III}(piv)_4\}_2(H_2O)\{W^V(CN)_8\}]$ was synthesized by introducing the cation, tetra (*n*-butyl)ammonium ion. The isolated mixed-metal system showed a ferrimagnetic behavior and the T_c value was estimated to be of 5.5 K from the ZFC and FC measurements. By comparison with the related complexes, the 2D sheet structure seems to be important to achieve high T_c value and the large coercive force. The mixed-metal systems containing ruthenium carboxylate and octacyanidotungstate are promising for constructing new magnetic materials.

4. Experimental section

4.1. General

Tetrafluoroborate of dinuclear ruthenium(II,III) and potassium octacyanidotungstate(IV) were prepared by a method described in the literature [11,25,33]. All of other reagents were commercially available and used as received.

4.2. Preparations

4.2.1. $[n\text{-}Bu_4N][\{Ru^{II}Ru^{III}(piv)_4\}_2(H_2O)\{W^V(CN)_8\}]\cdot 3H_2O$ (**1**$\cdot 3H_2O$)

To an aqueous solution (7 mL) of $K_4W(CN)_8\cdot 2H_2O$ (21 mg, 0.036 mmol), an aqueous solution (7 mL) of $[Ru_2(piv)_4(H_2O)_2]BF_4$ (30 mg, 0.036 mmol) and aqueous solution (7 mL) of *n*-Bu_4NCl (60 mg, 0.22 mmol) was added. The reaction mixture was stirred overnight in the dark, the resulting brown precipitate was filtered off, washed with water, and dried in vacuo. Yield, 30.4 mg (67%). Single crystals suitable for X-ray diffraction work were grown by slow diffusion of an aqueous solution in an H-shaped tube at room temperature in the dark. Anal. Calcd for $C_{64}H_{116}N_9O_{20}Ru_4W$: C, 40.04; H, 6.09; N, 6.57%. Found: C, 39.60; H, 5.81; N, 6.23%. IR (KBr, cm^{-1}): 2145 (vCN), 1488 (ν_{as}COO), 1420 (ν_sCOO). Diffuse reflectance spectra: λ_{max} 260, 368, 466, 540 (sh), 750 (sh), and 1100 (br) nm.

4.3. Physical techniques

FT-IR spectra were recorded using a JASCO MFT-2000 spectrophotometer with KBr pellets. Solid-state UV–vis spectra were recorded in the range of 200–1500 nm using a Shimadzu UV-3100 spectrophotometer (reflection method). Elemental analyses were performed using a Thermo Finnigan FLASH EA1112 analyzer. DC and AC magnetic data were measured using a Quantum Design MPMS XL SQUID magnetometer. The magnetic measurements were carried out at the University Claude Bernard Lyon 1 on polycrystalline samples. To avoid orientation in the magnetic field, the samples were pressed in a home-made Teflon sample holder equipped with a piston. The data were corrected for diamagnetism of the sample holder and the constituent atoms using Pascal's constants [34].

4.4. X-ray data collection and refinement

Diffraction data on single crystals of **1** were collected on a Bruker CCD X-ray diffractometer (SMART APEX) using graphite-monochromated Mo Kα radiation. Crystal data and details concerning the data collection are given in Table 1. The structure was solved by an intrinsic phasing method and refined by full-matrix least-squares methods. The C32 and C33 atoms were disordered into two positions (C32A and C32B, C33A and C33B), with occupation factors of 0.454 and 0.546, respectively. The hydrogen atoms, except for the water molecule, were inserted at their calculated positions, and fixed there. All of the calculations were carried out on a Windows 7 Core i7 computer using SHELXT-2014/4 and SHELXL-2014/7 [35,36]. Crystallographic data have been deposited with Cambridge Crystallographic Data Centre (Deposit number CCDC-1894536). Copies of the data can be obtained free of charge via http://www.ccdc.cam.ac.uk/conts/retrieving.html (or from the Cambridge Crystallographic Data Centre, 12, Union Road, Cambridge, CB2 1EZ, UK; Fax, +44 1223 336033; e-mail, deposit@ccdc.cam.ac.uk).

Acknowledgments

The present work was partially supported by Grant-in-Aid for Scientific Research Nos. 16K05722 and 17K05820 from the Ministry of Education, Culture, Sports, Science and Technology (MEXT, Japan) and the NEXT-Supported Program for the Strategic Research Foundation at Private Universities, 2010–2014.

Referencese

[1] F.A. Cotton, C.A. Murillo, R.A. Walton, Multiple Bonds between Metal Atoms, 3rd ed., Springer Science and Business Media, New York, 2005.
[2] M. Mikuriya, Bull. Jpn. Soc. Coord. Chem. 52 (2008) 17.
[3] M.A.S. Aquino, Coord. Chem. Rev. 248 (2004) 1025.
[4] M.A.S. Aquino, Coord. Chem. Rev. 170 (1998) 141.
[5] M. Mikuriya, D. Yoshioka, M. Handa, Coord. Chem. Rev. 250 (2006) 2194.
[6] Y. Sayama, M. Handa, M. Mikuriya, R. Nukada, I. Hiromitsu, K. Kasuga, in: G. Ondrejovic, A. Sirota (Eds.), Coordination Chemistry at the Turn of the Century, Slovak Technical University Press, Bratislava, 1999, p. 447.
[7] H. Ishida, M. Handa, M. Mikuriya, X-Ray Struct. Anal. Online 30 (2014) 9.
[8] Y. Hiraoka, T. Ikeue, H. Sakiyama, F. Guegan, D. Luneau, B. Gillon, I. Hiromitsu, D. Yoshioka, M. Mikuriya, Y. Kataoka, M. Handa, Dalton Trans. 44 (2015) 13439.
[9] H. Ishida, M. Handa, I. Hiromitsu, M. Mikuriya, Chem. J. Moldova. 4 (1) (2009) 90.
[10] H. Ishida, M. Handa, T. Ikeue, J. Taguchi, M. Mikuriya, Chem. Pap. 64 (2010) 767.
[11] Y. Sayama, M. Handa, M. Mikuriya, I. Hiromitsu, K. Kasuga, Bull. Chem. Soc. Jpn. 73 (2000) 2499.

[12] D. Yoshioka, M. Mikuriya, M. Handa, Bull. Chem. Soc. Jpn. 77 (2004) 2205.
[13] H. Ishida, M. Handa, I. Hiromitsu, M. Mikuriya, Chem. Pap. 67 (2013) 743.
[14] M. Handa, H. Ishida, K. Ito, T. Adachi, T. Ikeue, I. Hiromitsu, M. Mikuriya, K. Kasuga, Chem. Pap. 62 (2008) 410.
[15] D. Yoshioka, M. Handa, M. Mikuriya, I. Hiromitsu, K. Kasuga, Mater. Sci.-Poland 23 (2005) 765.
[16] D. Yoshioka, M. Handa, M. Mikuriya, K. Kasuga, in: M. Melnik, J. Sima, M. Tatarko (Eds.), Advances in Coordination, Bioinorganic and Inorganic Chemistry, Slovak Technical University Press, Bratislava, 2005, p. 218.
[17] D. Yoshioka, M. Mikuriya, M. Handa, Chem. Lett. 31 (2002) 1044.
[18] H. Ishida, M. Handa, I. Hiromitsu, S. Ujiie, D. Yoshioka, R. Mitsuhashi, M. Mikuriya, New J. Chem. 43 (2019) 1134.
[19] T.E. Vos, Y. Liao, W.W. Shum, J.-H. Her, P.W. Stephens, W.M. Reiff, J.S. Miller, J. Am. Chem. Soc. 126 (2004) 11630.
[20] T.E. Vos, J.S. Miller, Angew. Chem., Int. Ed. 44 (2005) 2416.
[21] J.S. Miller, Dalton Trans. 35 (2006) 2742.
[22] B.S. Kennon, K.H. Stone, P.W. Stephens, J.S. Miller, CrystEngChem (2009) 2185.
[23] J.-H. Her, P.W. Stephens, B.S. Kennon, C. Liu, J.S. Miller, Inorg. Chim. Acta 364 (2010) 172.
[24] D. Matoga, M. Mikuriya, M. Handa, J. Szklarzewicz, Chem. Lett. 34 (2005) 1550.
[25] M. Mikuriya, D. Yoshioka, A. Borta, D. Luneau, D. Matoga, J. Szklarzewicz, M. Handa, New J. Chem. 35 (2011) 1226.
[26] M. Mikuriya, Y. Tanaka, D. Yoshioka, M. Handa, Chem. J. Moldova. 9 (1) (2014) 93.
[27] M. Mikuriya, Y. Tanaka, D. Yoshioka, M. Handa, J. Supercond. Nov. Magnetism 28 (2015) 1013.
[28] M. Mikuriya, K. Ono, S. Kawauchi, D. Yoshioka, R. Mitsuhashi, M. Handa, Chem. J. Moldova 10 (2) (2015) 48.
[29] M. Mikuriya, S. Kawauchi, K. Ono, R. Mitsuhashi, N. Yoshinari, T. Konno, H. Tanaka, M. Handa, J. Supercond. Nov. Magnetism 30 (2017) 2007.
[30] M. Mikuriya, D. Yoshioka, R. Mitsuhashi, D. Luneau, D. Matoga, J. Szklarzewicz, M. Handa, Acta Phys. Pol. 131 (2017) 120.
[31] M. Mikuriya, S. Kawauchi, D. Yoshioka, R. Mitsuhashi, M. Handa, X-ray Struct. Anal. Online 34 (2018) 37.
[32] K. Nakamoto, Infrared and Raman Spectra of Inorganic and Coordination Compounds, Part B: Application in Coordination, Organometallic, and Bioinorganic Chemistry, 6th ed., John Wiley & Sons, Inc, New York, 2009.
[33] D. Matoga, J. Szklarzewicz, M. Mikuriya, Inorg. Chem. 45 (2006) 7100.
[34] O. Kahn, Molecular Magnetism, VCH publishers, New York, 1993.
[35] G.M. Sheldrick, Acta Crystallogr. C71 (2015) 3.
[36] G.M. Sheldrick, Acta Crystallogr. A64 (2008) 112.